

---

Articles

---

2022-06-10

## Fluorescent Calixarene-Schiff as a Nanovehicle with Biomedical Purposes

José Antonio Antonio Lebrón  
*University of Seville*

Manuel López-López  
*University of Huelva*

María Luisa Moyá  
*University of Seville*

*See next page for additional authors*

Follow this and additional works at: <https://arrow.tudublin.ie/creaart>

 Part of the [Life Sciences Commons](#)

---

### Recommended Citation

Lebrón JA, López-López M, Moyá ML, Deasy M, Muñoz-Wic A, García-Calderón CB, Valle Rosado I, López-Cornejo P, Bernal E, Ostos FJ. Fluorescent Calixarene-Schiff as a Nanovehicle with Biomedical Purposes. *Chemosensors*. 2022; 10(7):281. DOI: 10.3390/chemosensors10070281

This Article is brought to you for free and open access by ARROW@TU Dublin. It has been accepted for inclusion in Articles by an authorized administrator of ARROW@TU Dublin. For more information, please contact [arrow.admin@tudublin.ie](mailto:arrow.admin@tudublin.ie), [aisling.coyne@tudublin.ie](mailto:aisling.coyne@tudublin.ie), [gerard.connolly@tudublin.ie](mailto:gerard.connolly@tudublin.ie).



This work is licensed under a [Creative Commons Attribution-Noncommercial-Share Alike 4.0 License](#)


---

## Authors

José Antonio Antonio Lebrón, Manuel López-López, María Luisa Moyá, Mary Deasy, Ana Muñoz-Wic, Clara Beatriz García-Calderón, Iván Valle Rosado, Pilar López Cornejo, Eva Bernal Pérez, and Francisco José Ostos Marcos

## Article

# Fluorescent Calixarene-Schiff as a Nanovehicle with Biomedical Purposes

José Antonio Lebrón <sup>1</sup>, Manuel López-López <sup>2</sup>, María Luisa Moyá <sup>1</sup>, Mary Deasy <sup>3</sup>, Ana Muñoz-Wic <sup>1</sup>, Clara Beatriz García-Calderón <sup>4</sup>, Iván Valle Rosado <sup>4</sup>, Pilar López-Cornejo <sup>1,\*</sup>, Eva Bernal <sup>1,\*</sup> and Francisco José Ostos <sup>1,5,6,\*</sup>

- <sup>1</sup> Department of Physical Chemistry, Faculty of Chemistry, University of Seville, C/Profesor García González 1, 41012 Seville, Spain; jlebron@us.es (J.A.L.); moyá@us.es (M.L.M.); ana.munoz1@astrazeneca.com (A.M.-W.)
  - <sup>2</sup> Department of Chemical Engineering, Physical Chemistry and Materials Science, Faculty of Experimental Sciences, University of Huelva, Campus de El Carmen, Avda. de las Fuerzas Armadas s/n, 21071 Huelva, Spain; manuel.lopez@diq.uhu.es
  - <sup>3</sup> Centre of Applied Science for Health, Department of Applied Science, Technological University of Dublin, Tall13 laght, D24 FKT9 Dublin, Ireland; mary.deasy@tudublin.ie
  - <sup>4</sup> Institute of Biomedicine of Seville (IBiS), University Hospital Virgen del Rocío/CSIC/University of Seville, Avda. Manuel Siurot s/n, 41013 Seville, Spain; claragarcia@us.es (C.B.G.-C.); ivrosado@us.es (I.V.R.)
  - <sup>5</sup> Clinical Unit of Infectious Diseases and Microbiology, Institute of Biomedicine of Seville (IBiS), Virgen del Rocío University Hospital, CSIC, University of Seville, 41013 Seville, Spain
  - <sup>6</sup> Department of Medical Biochemistry, Molecular Biology and Immunology, School of Medicine, University of Seville, 41009 Seville, Spain
- \* Correspondence: pcornejo@us.es (P.L.-C.); evabernal@us.es (E.B.); fostos@us.es (F.J.O.); Tel.: +34-955421003 (P.L.-C.)



**Citation:** Lebrón, J.A.; López-López, M.; Moyá, M.L.; Deasy, M.; Muñoz-Wic, A.; García-Calderón, C.B.; Valle Rosado, I.; López-Cornejo, P.; Bernal, E.; Ostos, F.J. Fluorescent Calixarene-Schiff as a Nanovehicle with Biomedical Purposes. *Chemosensors* **2022**, *10*, 281. <https://doi.org/10.3390/chemosensors10070281>

Academic Editor: Guo-Hui Pan

Received: 10 June 2022

Accepted: 11 July 2022

Published: 14 July 2022

**Publisher's Note:** MDPI stays neutral with regard to jurisdictional claims in published maps and institutional affiliations.



**Copyright:** © 2022 by the authors. Licensee MDPI, Basel, Switzerland. This article is an open access article distributed under the terms and conditions of the Creative Commons Attribution (CC BY) license (<https://creativecommons.org/licenses/by/4.0/>).

**Abstract:** Gene therapy is a technique that is currently under expansion and development. Recent advances in genetic medicine have paved the way for a broader range of therapies and laid the groundwork for next-generation technologies. A terminally substituted difluorene-diester Schiff Base calix[4]arene has been studied in this work as possible nanovector to be used in gene therapy. Changes to luminescent behavior of the calixarene macrocycle are reported in the presence of ct-DNA. The calixarene macrocycle interacts with calf thymus DNA (ct-DNA), generating changes in its conformation. Partial double-strand denaturation is induced at low concentrations of the calixarene, resulting in compaction of the ct-DNA. However, interaction between calixarene molecules themselves takes place at high calixarene concentrations, favoring the decompaction of the polynucleotide. Based on cytotoxicity studies, the calixarene macrocycle investigated has the potential to be used as a nanovehicle and improve the therapeutic efficacy of pharmacological agents against tumors.

**Keywords:** calixarenes; ct-DNA; denaturation; compaction; gene therapy; nanocarriers

## 1. Introduction

Between the late 20th and early 21st centuries, 2335 gene therapy clinical trials were either completed ongoing, or approved worldwide. The number of clinical trials peaked in 2015, with a total of 163 trials. Most clinical trials of gene therapies have been conducted to treat specific cancerous diseases [1].

Gene therapy was designed to replace faulty genes or interrupt their expression. Following its successes and rapid development, there is a greater need for preparing highly efficient vectors, with low cytotoxicity, which can cross the cell membrane and the cytoplasm and release the genetic material into the cell nucleus. There are viral and non-viral vectors. Viral vectors often elicit an immune response in vivo, so researchers in recent years have focused more attention on non-viral vectors. These vectors bind to the polynucleotide, inducing a conformational change toward a more compact state. This phenomenon is called compaction or condensation. There is considerable documentation

in the bibliography on the use of cationic molecules to condense DNA and form complexes to facilitate gene transfer both *in vitro* and *in vivo* [2,3].

In recent years, many reviews have discussed the use of different macrocycles as non-viral vectors for gene transfection. Jiménez Blanco et al. [4] summarized the properties of preorganized macromolecular systems such as cyclodextrins, calixarenes, pillarenes, fullerenes, cyclopeptides, and cyclotrehalans, which are capable of self-assembling into nano-sized particles to allow a safe release of nucleic acids. Zhou et al. [5] reviewed the progress made in the condensation of ct-DNA molecules using nanostructure-based vectors and highlighted the elucidation of the complex structure formed with ct-DNA using different microscopic techniques. Rodik et al. [6] provided an overview of calixarenes, and related macrocycles, as vehicles in gene delivery, emphasizing the importance of having a preorganized scaffold incorporating alkyl chains in the structure. In that review, the authors pointed researchers to performing *in vivo* tests as a definitive step for evaluating the potential of these new materials in gene therapy products.

In relation to calixarenes, they can be functionalized with cationic groups on their upper rim and alkyl chains on their lower rim (or vice versa), thus making them promising vectors for the delivery of new genetic material. Multivalent platforms with guanidinium groups based on calixarenes have been used with great success in gene transfer. Sansone et al. [7] studied the capacity of these macrocycles in the binding, condensation, and transport of calf thymus DNA through cell membranes. In a systematic study, it was determined that the calix[4]arenes in the cone conformation lead to a more compact state of ct-DNA, due to the arrangement of their lipophilic chains. Additionally, an increase in the number of phenolic units in these receptors causes a partial compaction of the polynucleotide, as shown by AFM measurements. Calix[4]arenes in cone conformation only have been found to facilitate cell transfection effectively, which is indicative of a balance between hydrophobic and electrostatic interactions.

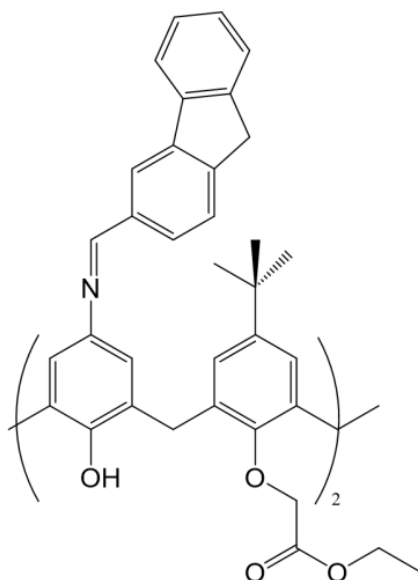
Rodik et al. [8] designed a protocol that optimized the ct-DNA compaction process in the presence of cationic amphiphilic calixarenes micelles, which were calix[4]arenes with choline groups and long hydrocarbon chains on their polar head. They generated aggregates of about 50 nm with suitable properties for transfection. In fact, efficient uptake of these vectors by adenocarcinoma cells from cervix/uterus (HeLa) was demonstrated by fluorescence microscopy [8]. In a later study, they further improved the polynucleotide condensation process by lengthening the alkyl chains, which led to smaller aggregates with low polydispersity index, thus promoting more efficiently gene transfection and decreasing cytotoxicity. On the other hand, it was observed that changes in the nature of the groups at the polar head do not play a fundamental role in this process.

With the aim of increasing the cooperativity phenomenon, Lalor et al. [9] prepared functionalized cationic multi-calixarenes, where one calix[4]arene acted as the central unit of the superstructure, which also contained four other calix[4]arene molecules, linked by short polar spacer groups. Each terminal macrocycle has a glycine residue with a free aliphatic amine at its upper terminus. Binding between multimeric calixarenes and ct-DNA was observed at lower macrocycle concentrations than when binding to a single calixarene structure, pointing to a cooperative effect. Furthermore, cytotoxicity for different cell lines was negligible and gene transfection was confirmed in Chinese hamster ovary (CHO) cells.

Rallaud et al. [10] demonstrated that not only electrostatic-type interactions take place between cationic calixarenes and ct-DNA, but there may also be interactions with the major or minor groove of the polynucleotide. For this purpose, they used amphiphilic calix[4]arenes functionalized with guanidinium groups. It was observed that dimers of these calixarenes interact with the polynucleotide, inducing conformational changes through interactions with the major groove of ct-DNA. These changes depended on the structure of the macrocycle [11,12].

In this work, the interaction of a Schiff-Base calix[4]arene with calf thymus DNA has been studied. The calixarene investigated has a terminal ester group on the lower rim and an ortho fused polycyclic arene group in the upper rim (see Scheme 1), with nucleic

acid binding capacity. Several techniques were used to determine its binding ability with a polynucleotide. Results have shown that this macrocycle is a potential candidate for healthcare applications.



**Scheme 1.** Structure of the calix[4]arene investigated in this work (5,17-(9H-fluoren-2-yl) methyleneamino-11,23-di-tert-butyl-25,27-diethoxycarbonyl methyleneoxy-26,28-dihydroxycalix[4]arene ( $C_{72}H_{70}N_2O_8 \cdot H_2O$ )).

## 2. Materials and Methods

### 2.1. Materials

Ethidium bromide and sodium cacodylate were purchased from Sigma-Aldrich (Darmstadt, Germany). The polynucleotide calf thymus DNA sodium salt (double stranded ct-DNA, ds-DNA) was obtained from Fluka (Darmstadt, Germany) and also used without further purification. Ct-DNA concentration, as measured by phosphate groups, was determined spectrophotometrically from molar absorptivity ( $6600 \text{ mol}^{-1} \cdot \text{dm}^3 \cdot \text{cm}^{-1}$  at 258 nm) [13]. An agarose gel electrophoresis test using ethidium bromide indicated that the average number of base pairs per ct-DNA molecule is above 10,000 bp [14]. The ratios in absorbance measured at 260 and 280 nm of the solutions were found to be between 1.8 and 1.9, suggesting the absence of proteins [15]. The 5,17-(9H-fluoren-2-yl)methyleneamino-11,23-di-tert-butyl-25,27-diethoxycarbonyl methyleneoxy-26,28-dihydroxycalix[4]arene was synthesized as described previously (Scheme 1) [16]. This calixarene is poorly soluble in water due to the hydrophobic nature of this macrocycle, but it was soluble in a mixture of methanol/water at 20% (*v/v*). All experiments were carry out at this methanol/water mixture. Methanol was supplied from Merck (Darmstadt, Germany). Some measurements were also carried out with simple stranded ct-DNA (ss-DNA) to help the discussion of the results. For this purpose, ss-DNA stock solutions were prepared by thermal denaturalization of ds-DNA following the procedure given in the literature [17]. All solutions were prepared with deionized water from a Millipore Milli-Q system, having a conductivity  $<10^{-6} \text{ Sm}^{-1}$ . The measurements were done at a fixed temperature of  $298.2 \pm 0.1 \text{ K}$  and at a fixed pH using a buffer solution ( $[\text{cacodylate}] = 0.01 \text{ mol} \cdot \text{dm}^{-3}$ , pH = 7.0).

### 2.2. Methods

#### 2.2.1. Absorbance Measurements

Absorbance spectra were obtained at different X values ( $X = [\text{calixarene}]/[\text{ct-DNA}]$ ) to check the stability of the calixarene/ct-DNA solutions. A CARY 500 SCAN UV-vis-NIR spectrophotomer (Varian) was used. The spectra were recorded in the wavelength range

from 200 to 800 nm and data were collected every 2 nm. A standard quartz cell of 10 mm path length was used. The ct-DNA concentration used was  $2.00 \times 10^{-5} \text{ mol}\cdot\text{dm}^{-3}$ .

### 2.2.2. Fluorescence Measurements

Fluorescence emission intensity measurements were carried out using a Hitachi-F-2500 spectrofluorimeter interfaced to a PC for the recording and handling of the spectra. A standard quartz cell of 10 mm path length was used. Fluorescence titrations were performed at a fixed calixarene concentration of  $2.00 \times 10^{-6} \text{ mol}\cdot\text{dm}^{-3}$ ; and variable ct-DNA concentrations in the mole ratio range of  $X = 0$  to 0.2. Experiments at  $X$  values higher than 0.2 were not carried out due to calixarene solubility problems. The excitation and emission wavelengths were 318 nm and 410 nm, which were the maximum wavelengths corresponding to the calixarene. Both emission and excitation slits were equal to 10 nm.

### 2.2.3. Circular Dichroism Spectra

Electronic circular dichroism (CD) spectra were recorded using a Biologic Mos-450 spectropolarimeter. A standard quartz cell of 10 mm path length was used. Scans were taken from 220 to 320 nm for the intrinsic region. Each spectrum was obtained from an average of 10 runs at a fixed temperature of 298.2 K, with a 5 min equilibration before each scan. The results obtained were expressed in terms of molar ellipticity.

Spectra were registered at a fixed ct-DNA concentration and varying amounts of calixarene to obtain the appropriate molar ratio  $X$  ( $X = [\text{calixarene}]/[\text{ct-DNA}]$ ).

### 2.2.4. Viscosity Measurements

Viscosity measurements were carried out using an Ostwald microviscometer, calibrated for water and methanol, immersed in a thermostated water bath at a temperature of  $298.2 \pm 0.1 \text{ K}$ . Each measurement was repeated at least ten times. The viscosity of the ct-DNA–calixarene solutions was expressed as the relative viscosity  $\eta_r$ , defined as  $\eta/\eta_0$ ; that is, the ratio between the viscosity of the working solution and the viscosity of the pure solvent (methanol/water at pH = 7 with a sodium cacodylate buffer).

### 2.2.5. Melting Measurements

The thermal denaturalization study was performed on a Biologic spectrophotometer equipped with a Peltier temperature controller, which permitted the control of the speed at which temperature changes during the experiments. The rise in temperature was  $0.2 \text{ }^\circ\text{C min}^{-1}$ . The recording chart read temperature and absorbance differences between the reference and the sample cuvettes at 260 nm.

All melting measurements were performed at a fixed ct-DNA concentration of  $1.20 \times 10^{-5} \text{ mol}\cdot\text{dm}^{-3}$ .

### 2.2.6. AFM Measurements

The images were obtained with a Molecular Imaging PicoPlus2500 AFM (Agilent Technologies). Silicon cantilevers (Model Point-probe, Nanoworld) with a resonance frequency of around 240 kHz and nominal force constant of 42 N/m were used. All AFM imaging were recorded in air and in tapping mode, with scan speeds of about 0.5 Hz, with data collection at  $256 \times 256$  pixels.

Due to the large size of ct-DNA, dilute solutions ( $0.3 \text{ } \mu\text{mol dm}^{-3}$ ) were used to image isolated ct-DNA molecules. AFM images were obtained by drying 30  $\mu\text{L}$  of calixarene and ct-DNA solution previously deposited on a modified mica surface. This surface was prepared by dropping a 0.1% ( $v/v$ ) APTES aqueous solution onto a freshly cleaved mica surface. The surface was washed with ultra-pure water and air dried after 20 min. The calixarene/ct-DNA solution dropped onto the modified surface was incubated for 30 min, washed with pure water, and air dried prior to AFM imaging.

### 2.2.7. In Vitro Cytotoxicity Assays

Cytotoxicity was investigated at calixarene concentrations from 0 to  $2.56 \mu\text{mol dm}^{-3}$ . An MTT assay was used for in vitro results [18]. Calixarene concentrations higher than  $2.56 \mu\text{mol dm}^{-3}$  could not be used due to their poor solubility. The cell lines used were RPE-1 (normal cell line), HepG2 (human liver cancer cell line), A549 (adenocarcinomic human alveolar basal epithelial cell line), MCF7 (breast cancer cell line), and LS180 (adenocarcinomic human colonic epithelial cell line), and received from the IBiS (the Institute of Biomedicine of Seville) which were from commercial suppliers. Cell lines were plated out into 96-well plates at a density of 3000 cells per plate and incubated. After 24 h, different calixarene solutions of varying concentrations were added to the wells, and the plate was returned to the incubator for 2 more days. Subsequently, they were pulsed with MTS (ROCHE, Basilea, Switzerland). Cell viability was measured by luminometry in a Varioskan Flash (Thermo Fisher Scientific, Waltham, MA, USA) in accordance with the manufacturer instructions. Each calixarene concentration was measured in triplicate.

## 3. Results and Discussion

Figure 1 shows the stability of calix[4]arene/ct-DNA solutions for an  $X$  value of 0.008 for the Schiff Base calixarene. Similar results were obtained for other  $X$  values. The calixarene/ct-DNA solutions have a stability of more than two hours within the range of concentrations studied.

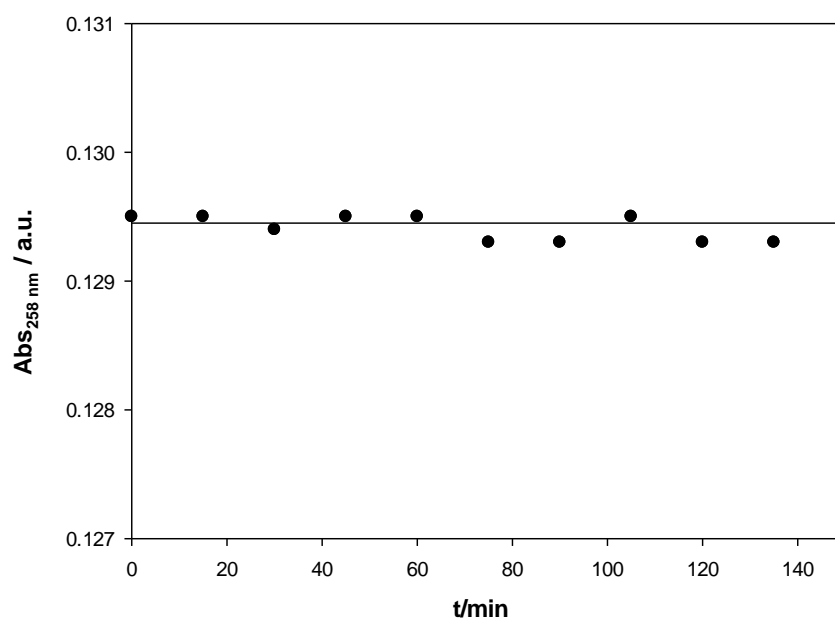


**Figure 1.** Stability of a calixarene/ct-DNA solution ( $X = 0.008$  and  $[\text{ct-DNA}] = 2.00 \times 10^{-5} \text{ mol}\cdot\text{dm}^{-3}$ ).

Fluorescence emission spectroscopy is a technique frequently used to obtain information about the binding mode of different species to ct-DNA. Normally, the interaction of a fluorescent compound with ct-DNA leads to changes in the emission spectrum of the dye [19]. The calixarene functionalized with fluorene groups exhibits a fluorescence emission spectrum with a maximum at a wavelength of 410 nm when it is irradiated at 318 nm. This characteristic allows extracting information about the Schiff Base calixarene/ct-DNA complex, without the need to add any other probe such as ethidium bromide. Figure 2 shows the dependence of the calixarene-ct-DNA solutions fluorescence emission intensity (EI), at 410 nm, on the molar ratio  $X$ . The results obtained demonstrate that, at small  $X$  values, there is a decrease in the emission intensity when the DNA concentration increases. However, from a value around  $X = 0.005$ , the emission intensity began to increase until it reached a more or less constant value. No shift in the emission band of the macrocycle was observed. Therefore, the fluorescence was due to the excitation of two polycyclic aromatic

groups (present in the fluorine groups) in the calixarene structure. These groups have a planar symmetry, so it is possible that they are intercalated between the base pairs of the polynucleotide. In fact, this intercalation could explain the observed decrease in the emission intensity at low  $X$  values, since a change in the hydrophobic environment of the fluorene groups could cause a decrease in the EI. As the value of  $X$  increases, the emission intensity also increases. This observation may be due to the formation of calixarene dimers at the fluorine sites in the structure, when the polynucleotide concentration diminishes. The formation of calixarene dimers due to  $\pi$ - $\pi$  type interactions between aromatic rings has previously been shown in the literature for this compound [16]. The appearance of these dimers would imply changes in the intensity of the fluorescence emission, not only because the environment of the emitting molecules can change, but also because it could reverse the equilibrium of the calixarene/ct-DNA complex formation, favoring calixarene-calixarene interactions and, thus, weakening the calixarene-ct-DNA interactions.

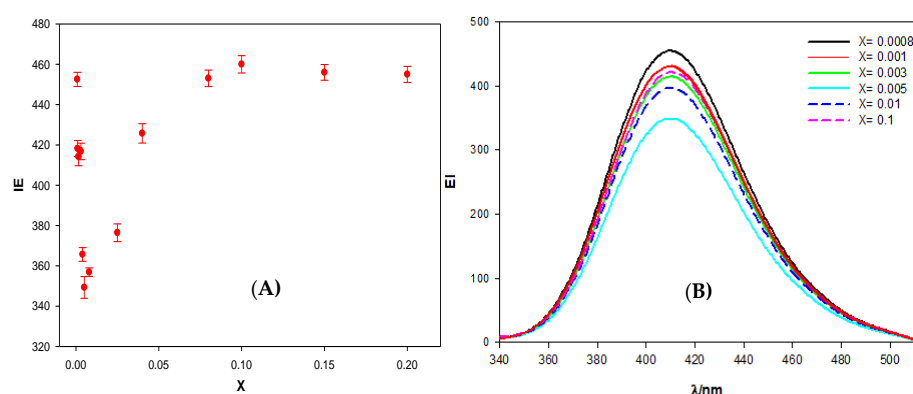
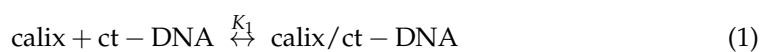


**Figure 2.** (A) Representation of the fluorescence emission intensity of Schiff Base calixarene/ct-DNA solutions on  $X$ , at a fixed macrocycle concentration ( $[\text{calixarene}] = 2.00 \times 10^{-6} \text{ mol}\cdot\text{dm}^{-3}$ ). Error bars represent the standard deviation for each  $X$  value ( $n = 5$ ). (B) Emission spectrum of the difluorene-diester calixarene at different  $X$  values.

The first decrease observed in Figure 2 allowed for the quantification of the binding between the Schiff Base calixarene with ct-DNA. This measurement was made using the Two-State Model (also known as Pseudophase Model), proposed by Menger and Portnoy [20], in which two possible states for the macrocycle are considered: one in the free state and one bound to the polynucleotide (Equation (1)):

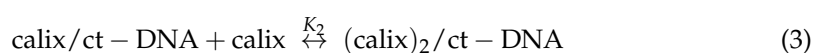


Considering this two-state distribution for the calixarene, one can write the following equation:

$$\frac{I}{I_0} = \frac{\left(\frac{I}{I_0}\right)_w + K_1 \left(\frac{I}{I_0}\right)_b [\text{DNA}]}{1 + K_1 [\text{DNA}]} \quad (2)$$

where  $I$  and  $I_0$  are the fluorescence emission intensities of the difluorene-calixarene measured in the presence and absence of DNA, respectively;  $(I/I_0)_w$  is the relative emission intensity of the calixarene located in the aqueous solution and  $(I/I_0)_b$  the relative emission intensity of the bound calixarene; that is, that of the calixarene-ct-DNA complex [21].

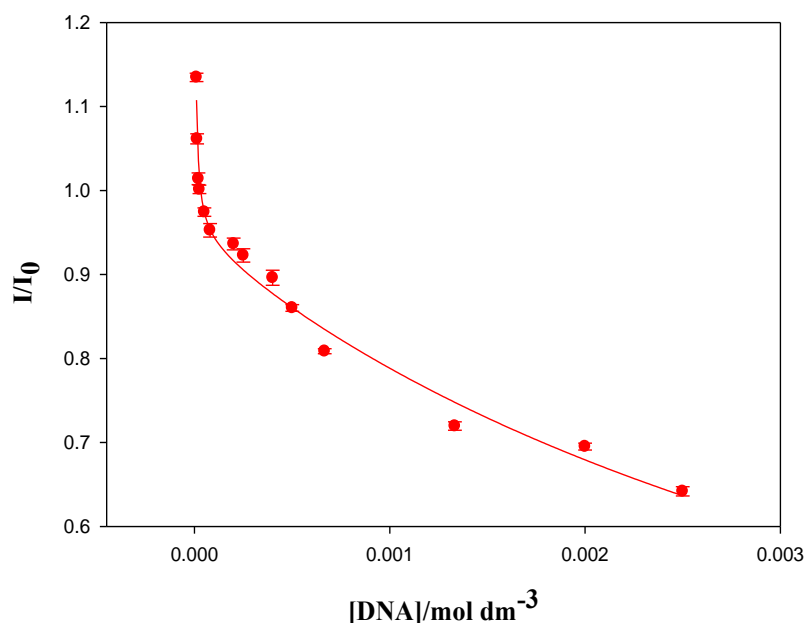
Equation (2) does not explain or fit the experimental data in the  $X$  range 0–0.005. Bearing in mind the structural characteristics of the calixarene macrocycle, the formation of dimers at the surface of the polynucleotide must be considered. Therefore, the equilibrium must be taken into account in Equation (2), resulting in the following equation:





$$\frac{I}{I_0} = \frac{\left(\frac{I}{I_0}\right)_w + K_1\left(\frac{I}{I_0}\right)_1[\text{DNA}] + K_1K_2\left(\frac{I}{I_0}\right)_2[\text{DNA}]^2}{1 + K_1[\text{DNA}] + K_1K_2[\text{DNA}]^2} \quad (4)$$

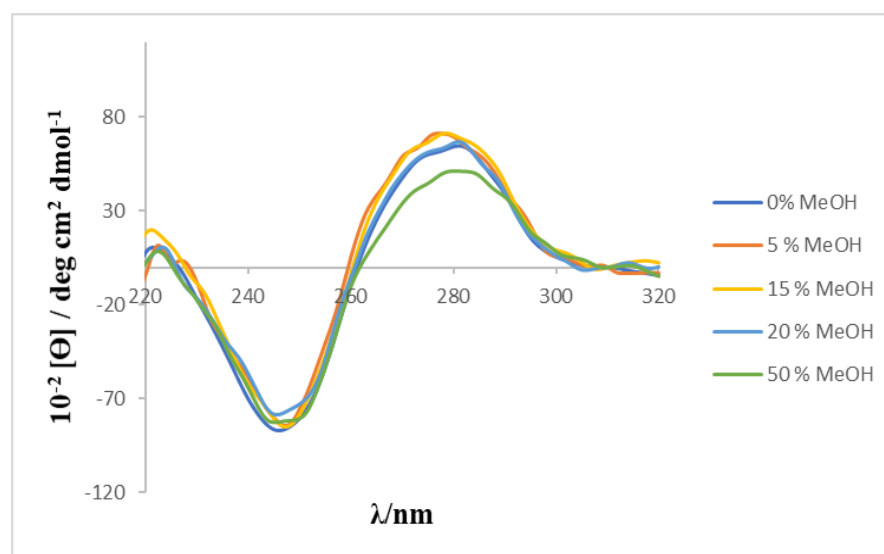
where  $(I/I_0)_w$ ,  $(I/I_0)_1$ , and  $(I/I_0)_2$  are the free and fully bound relative fluorescence emission intensities, for processes 1 and 3, respectively.  $K_1$  and  $K_2$  are the equilibrium constants of these equilibria. The experimental results shown in Figure 3 were fitted by using Equation (4). These values correspond to data obtained in the range of  $X = 0$ – $0.005$  and as shown in Figure 3. A good agreement between the experimental and the theoretical data was observed and, from the fitting, the binding constants  $K_1 = 2.8 \times 10^5 \text{ mol}^{-1}\text{dm}^3$  and  $K_2 = 219 \text{ mol}^{-1}\text{dm}^3$  were obtained. This  $K_1$  value agrees with those obtained by Zadmard et al. in the study of the association processes of calixarene dimers with different double-stranded nucleic acids [11].



**Figure 3.** Dependence of the  $I/I_0$  ratio of the difluorene-calixarene diester/ct-DNA solution on the polynucleotide concentration ( $[\text{calixarene}] = 2.00 \times 10^{-6} \text{ mol}\cdot\text{dm}^{-3}$ ). The solid line corresponds to the multiparameter fit obtained using Equation (4). Error bars represent the standard deviation for each polynucleotide concentration value ( $n = 5$ ).

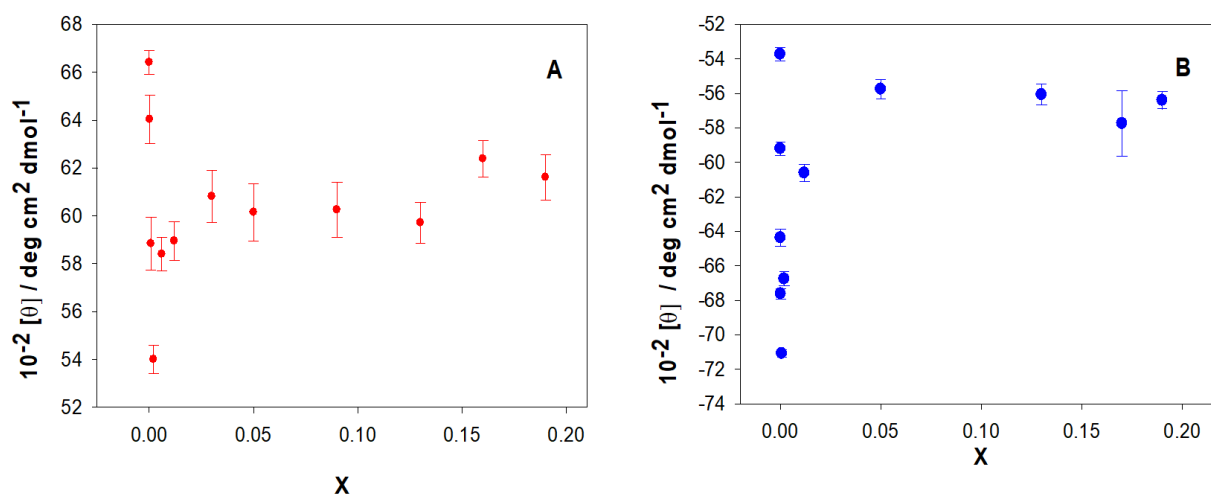
To further investigate the interactions between the Schiff Base calixarene and the ct-DNA, circular dichroism (CD) measurements were performed at different  $X$  values.

Circular dichroism spectra of calixarene-ct-DNA solutions were carried out at a constant polynucleotide concentration and different macrocycle concentrations. These studies were intended to determine possible conformational changes in the ct-DNA molecules due to their interactions with the calixarene. ct-DNA in aqueous solution adopts a right-handed B-form conformation, showing a characteristic CD spectrum in the near ultraviolet region (220–320 nm). The spectrum showed a positive band at approximately 278 nm and a negative one at 247 nm. These bands are caused, respectively, by the  $\pi$ – $\pi$  stacking interactions between the base pairs and by the helical superstructure of the polynucleotide that generates an asymmetric environment for the bases [22]. The conformational alterations of ct-DNA, caused by its interaction with different ligands, produces changes in its CD spectrum [23,24]. Given that a MeOH/ $\text{H}_2\text{O}$  mixture was used as solvent because of the low solubility of the calixarene, a preliminary study was carried out to check the effect of the MeOH percentage on the CD spectrum of ct-DNA. The results (see Figure 4) showed that the characteristic bands of the CD spectrum of ct-DNA do not undergo any modification in the presence of the content of alcohol used in the present work.



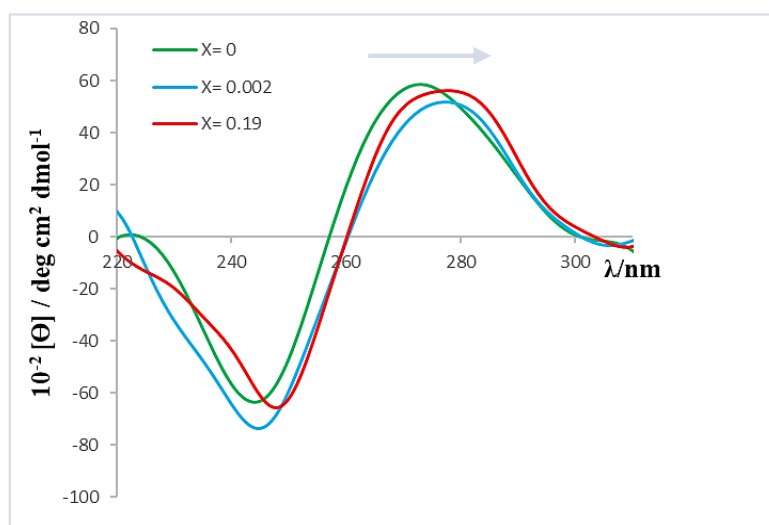
**Figure 4.** Circular dichroism spectrum of ct-DNA at different MeOH/water volume ratios ( $[ct-DNA] = 2.00 \times 10^{-5} \text{ mol}\cdot\text{dm}^{-3}$ ).

Figure 5 shows the molar ellipticity dependence of the positive and negative bands of the ct-DNA CD spectrum on the X value.



**Figure 5.** Dependence of the molar ellipticity of the positive (A) and negative (B) bands on the molar ratio X ( $[ct-DNA] = 2.00 \times 10^{-5} \text{ mol}\cdot\text{dm}^{-3}$ ). Error bars represent the standard deviation for each X value ( $n = 10$ ).

As can be seen, the molar ellipticity of both bands decreases within the range  $0 < X < 0.002$ . In addition, although the profile or shape of the spectrum remained constant throughout the range of X values studied, the bands showed a bathochromic shift of approximately 3 nm when X increased (see Figure 6). This observed shift could be related to the polynucleotide denaturation; that is, the separation of the ct-DNA double helix, resulting in two single-stranded ct-DNA molecules [17]. Since the ct-DNA chains are held together by hydrogen bonds between complementary base pairs, a possible intercalation of the macrocycles between them could disrupt the hydrogen bond between the base pairs thereby affecting the spectrum. Another possibility, mentioned previously, is the potential formation of calixarene dimers which may also affect the conformation of ct-DNA. To obtain additional information on this issue, viscosity and melting temperature measurements were performed.



**Figure 6.** Circular dichroism spectrum of ct-DNA at different values of  $X$ . The inset shows the dependence of the inflection point on  $X$ . [ct-DNA] =  $2.00 \times 10^{-5}$  mol·dm $^{-3}$ ).

Information on the macroscopic properties of microheterogeneous systems can be obtained from viscosity measurements [25]. In fact, with respect to ct-DNA solutions, the different binding modes of a ligand to the polynucleotide can be distinguished. If the calixarene ligand and the polynucleotide interact in a way that causes separation of the ct-DNA strands, this would result in an increase in the viscosity of the solution [25]. Conversely, if a groove-type or an electrostatic binding occurs, no changes in viscosity would be expected [26]. In addition, if the interactions cause morphological changes in the polynucleotide, then these can affect the viscosity. For example, if the ct-DNA is compacted, a decrease in the viscosity is expected. Figure 7A shows the dependence of the relative viscosity,  $\eta_r$ , on the molar ratio  $X$  for the macrocycle studied. As can be seen,  $\eta_r$  increases at low values of  $X$  and subsequently decreases with increasing the macrocycle concentration, at a fixed ct-DNA concentration. The maximum was observed at an  $X$  value of  $\sim 0.003$ .

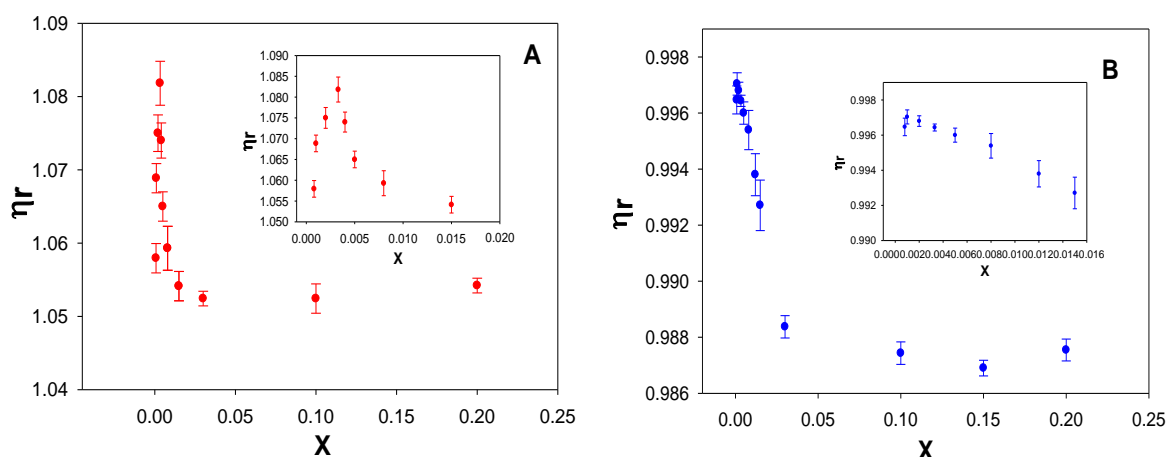


**Figure 7.** Relative viscosity of the calixarene/ds-DNA (A) and calixarene/ss-DNA (B) solutions at different values of  $X$  ([DNA] =  $2.00 \times 10^{-5}$  mol dm $^{-3}$ ). Inserts show the relative viscosity data at low  $X$  values. Error bars represent the standard deviation for each value of  $X$  ( $n = 10$ ).

The initial increase in viscosity could correspond to a denaturation of the double-stranded ct-DNA, due to the calixarene/ct-DNA interactions. To investigate this possibility, the viscosity of calixarene/ss-DNA solutions was investigated (Figure 7B). In this case, a constancy of viscosity was observed in the range of  $X$  from 0 to 0.003.

Subsequently, the relative viscosity of the ct-DNA solution decreased with increasing concentration of the macrocycle, as occurred with the double stranded ct-DNA. The explanation for this behavior will be provided later. The results suggest that polynucleotide denaturation occurs at low X values due to the calixarene/DNA interaction.

To gain further information about how the calixarene molecules interact with ct-DNA, measurements of the melting temperature,  $T_m$ , were performed. This temperature was determined as the average of the initial and final temperatures corresponding to the melting process. The profiles were sigmoidal for all X values studied (Figure 8). The ct-DNA melting transition was highly cooperative ( $\Delta T \approx 10\text{--}15\text{ }^\circ\text{C}$ , see Figure 8A,B,D–F). However, a less cooperative trend was obtained for  $X = 0.003$  for the Schiff Base calixarene ( $\Delta T \approx 30\text{ }^\circ\text{C}$ , see Figure 8C). A less cooperative transition happens if a partial opening of the double helix takes place, which would be accompanied by a decrease in  $T_m$ , in agreement with the experimental observations.

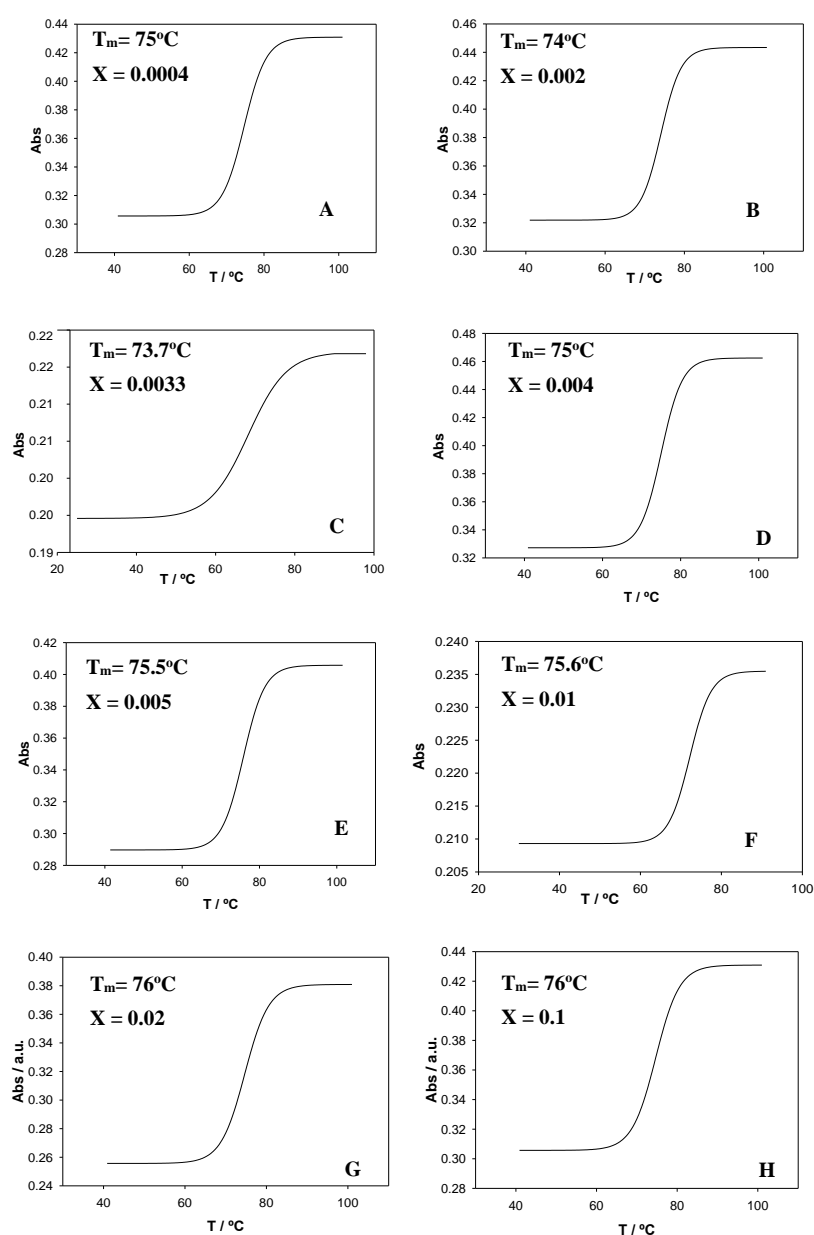


**Figure 8.** (A–H) Melting profiles obtained at different molar ratios of X for calixarene/ct-DNA solutions ( $[\text{ct-DNA}] = 1.20 \times 10^{-5} \text{ mol}\cdot\text{dm}^{-3}$ ).

Figure 9 shows the dependence of  $T_m$  on the molar ratio  $X$ . An initial decrease in melting temperature was observed in the range of  $X$  from 0 to 0.003. A further increase in  $X$  resulted in an increase in  $T_m$ . It is seen that the values of  $X$  where a minimum point of  $T_m$  was observed coincided with those observed from the viscosity measurements.

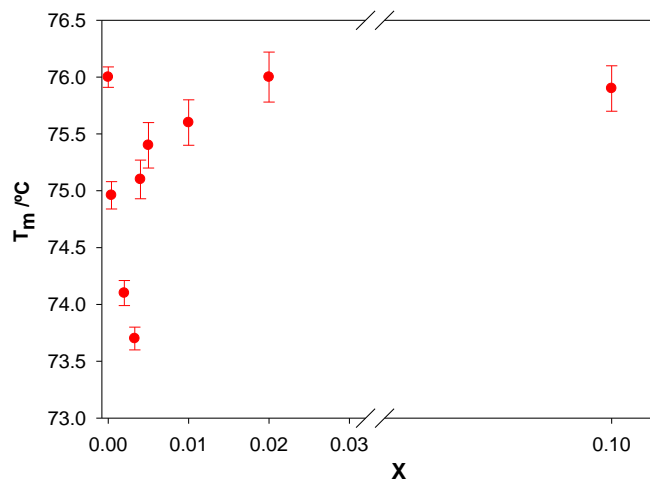


**Figure 9.** Melting temperature values obtained at different  $X$  values for the calixarene/ct-DNA solutions ( $[ct-DNA] = 1.20 \times 10^{-5} \text{ mol}\cdot\text{dm}^{-3}$ ). Error bars represent the standard deviation for each value of  $X$  ( $n = 3$ ).

When a ligand intercalates between the base pairs of the polynucleotide, without affecting the separation of the double helix, an increase in the rigidity of the ct-DNA double helix and a prevalence of the B form happen [27]. This would result in an increase in  $T_m$  and could be accompanied by conformational changes in the polynucleotide. Fluorene groups (and derivatives) are known to interact with ct-DNA by intercalation between the base pairs of the polynucleotide [28,29]. Thus, the calixarene could be intercalated into the ct-DNA backbone through the fluorene groups. Since an initial decrease in the melting temperature was observed at low  $X$  molar ratios, the interaction of the calixarene with the polynucleotide would most likely occur via a groove-type interaction, causing the breaking of the hydrogen bonds between the base pairs and destabilization of the double helix due to a partial separation of the double strand. This type of behavior has been previously observed for other species. For example,  $\text{Cu}^{2+}$  ions induce a break in the hydrogen bonds between guanine and cytosine, leading to a destabilization of the double helix [30]. Other ions such as  $\text{Zn}^{2+}$ ,  $\text{Mn}^{2+}$ ,  $\text{Ni}^{2+}$ , and  $\text{Co}^{2+}$  also cause destabilization of the double ct-DNA helix at high concentrations [31]. The increase in the melting temperature observed for  $X > 0.003$  suggests changes in ct-DNA conformation.

Supian et al. observed that calixarene aggregates were formed in the solid state for Schiff Base calix[4]arenes, in which the molecules stack one inside the other [16,32]. Therefore, supramolecular aggregates may have formed in solution for this calixarene ligand. The formation of these aggregates would be favored at high macrocycle concentrations.

Thus, the behavior observed in our studies here using many techniques for  $X$  values  $> 0.003$  may be due to the formation of supramolecular aggregates in the solution, which would be favored by increasing the concentration of the macrocycle. If such aggregates stabilize the calixarene molecules in the aqueous solution, the addition of more calixarene to the medium would weaken the calixarene/ct-DNA interactions. The released polynucleotide molecules would then revert to a more extended conformation, similar to the initial one.

To obtain information on the structure of the calixarene/ct-DNA complexes, atomic force microscopy (AFM) measurements were performed. Figure 10 shows the results obtained. In the absence of calixarene, the typical elongated form of the ct-DNA molecules was observed. At low  $X$  values, the macrocycle interacts with the polynucleotide, inducing an increase in the bending of the ct-DNA molecules. This increase results in a decrease in

the length persistence, which leads to the formation and stabilization of intramolecular loops (see Figure 10A,B). Here, stabilization occurs by the formation of flower- and disc-like structures, which are considered to be a type of strand-with-strand stabilization, as reported by Fang and Hoh [33,34]. For  $X > 0.003$ , a structural change of the polynucleotide from a more compact (partial) state to a more extended structure is observed. Hence, a decompaction process was produced, as evident from Figure 10C,D. The compact structures appear to be further apart, perhaps due to the loss of loops. Pearl-ring structures appear. This new arrangement of the polynucleotide could be due to the stacking of the calixarene molecules in solution, to form aggregates (as can be seen in Figure 2 at values of  $X > 0.003$ ), which would ultimately produce a weakening of the interactions between the calixarene and the ct-DNA. Therefore, a less compact structure would occur which agrees with the results found from the other techniques.

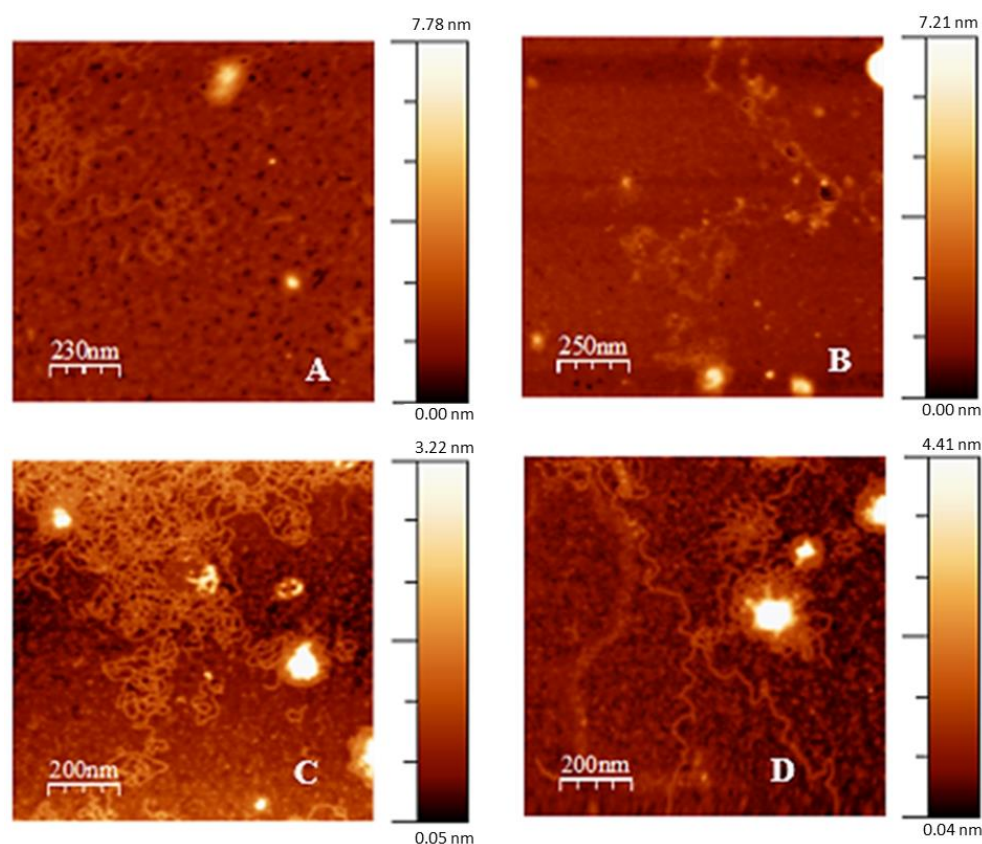


**Figure 10.** AFM topographic image of calf thymus ct-DNA adsorbed on an APTES-modified mica surface in the presence of the Schiff Base calixarene ((A)  $X = 0.0008$ , (B)  $X = 0.003$ , (C)  $X = 0.1$  and (D)  $X = 0.2$ ).

The formation of supramolecular structures has been demonstrated by fluorescence measurements. The Schiff Base calixarene showed two emission bands at 410 and 638 nm when excited at 318 nm. The emission spectrum was recorded in a MeOH/water solution (20% water/MeOH (*v/v*), pH = 7.0 with 0.01 M cacodylate) at different macrocycle concentrations. The results are shown in Figure 11, and a linear increase in the emission intensity is observed with increasing calixarene concentration. However, from a particular concentration value, a change in the slope is seen. This abrupt change in the trend of the fluorescence emission is most likely related to the formation of supramolecular aggregates. An increase in the hydrophobic nature of the macrocycle environment can result in early formation of supramolecular aggregates.

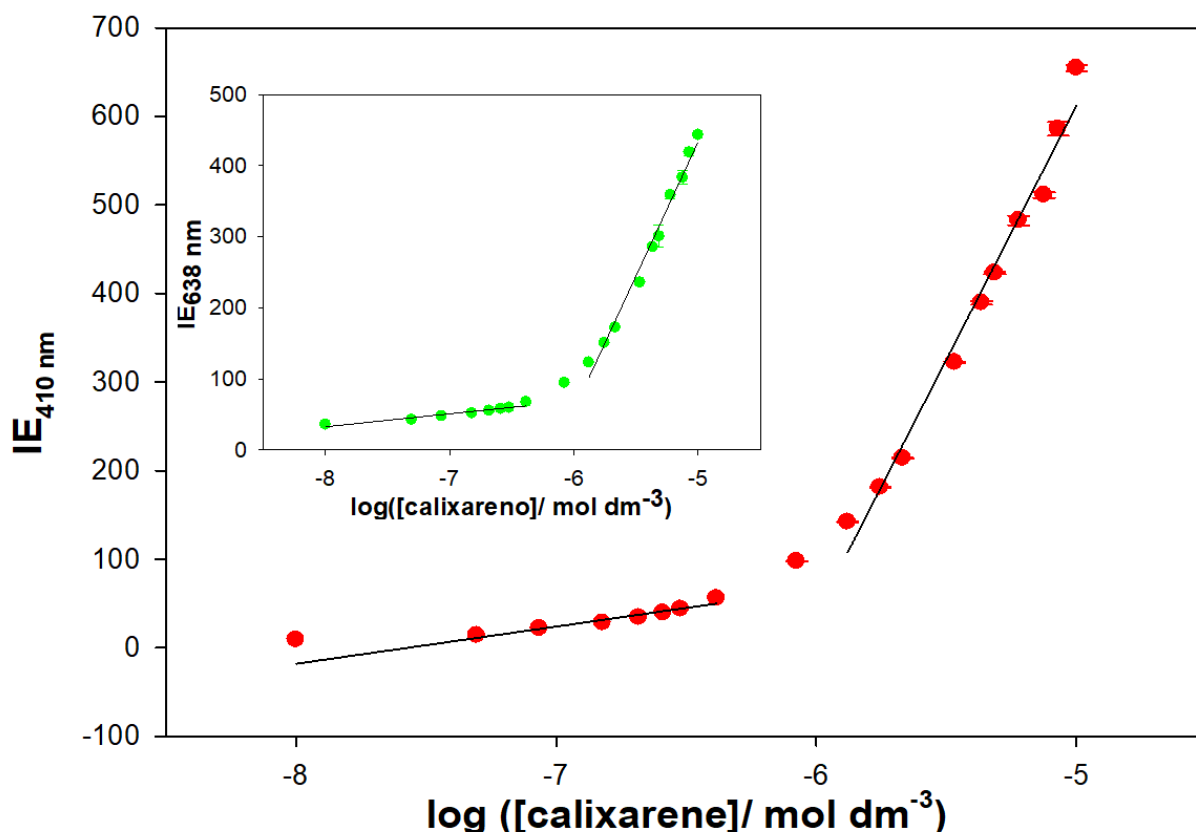


**Figure 11.** Emission intensity Schiff Base calixarene ( $\lambda_{\text{exc}} = 318$  nm,  $\lambda_{\text{em}} = 410$ , and 638 nm) in aqueous solution at different concentrations of the macrocycle. Error bars represent the standard deviation for each calixarene concentration value ( $n = 5$ ).

The results obtained in this work have been compared with those previously obtained by our research group in the study of cationic surfactants as vectors for ct-DNA condensation [35,36]. For example, cetyltrimethylammonium bromide (CTAB) or dimeric surfactants (12-2-12,2Br- and 12-10-12,2Br-) cause compaction of the polynucleotide. The electrostatic interaction between the cationic head of the surfactants and the phosphate groups of the ct-DNA, as well as the hydrophobic interactions between the hydrocarbon chains of the surfactant molecules that are located at the surface of the polynucleotide, are responsible for compaction. However, by increasing the concentration of the surfactant, decompaction of the ct-DNA was observed. This behavior was explained based on the formation of micelles in the solution. The calixarene studied also induces compaction of the polynucleotide. However, its mode of binding to ct-DNA is different. Before causing a conformational change in the ct-DNA, this calixarene interacts with the polynucleotide through a groove-type binding mode, which induces the breaking of the hydrogen bond between the base pairs and, therefore, leads to a partial denaturation of the double helix. This is in agreement with the results previously obtained and favors the condensation process. As was the case for the surfactants, above a certain concentration of calixarene, a decompaction of the polynucleotide takes place. The formation of supramolecular structures between the molecules of the macrocycle in solution favors the breakage of the compact ct-DNA globules.

Given that the goal of the work was to investigate the potential of the Schiff Base calixarene as a vector, it is essential to examine the viability of various cell lines in the presence of different calixarene concentrations. With this in mind, the cytotoxic effect that the macrocycle exerts on different cell lines was measured. These studies were performed over a 48-h time period. The results are shown in Figure 12.



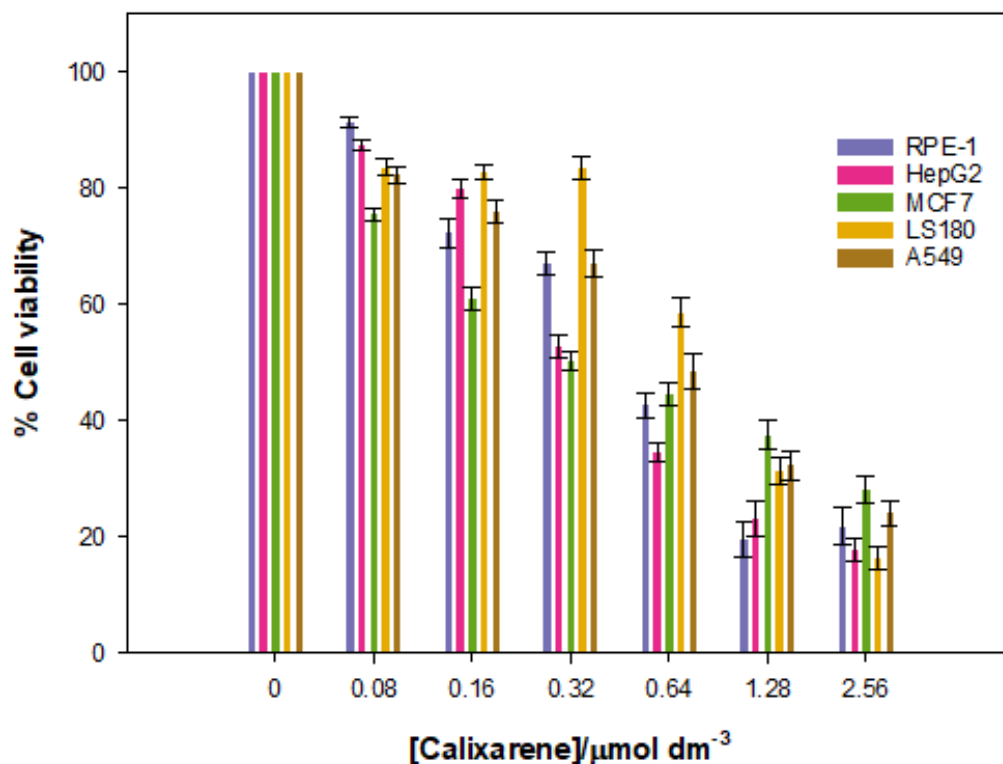


**Figure 12.** % Cell viability in the presence of different amounts of the Schiff Base calixarene for different cell lines during a period of 48 h.

The data show a low cytotoxicity for cancerous lines, especially at low concentrations of calixarene, but the cell viability decreased at higher concentrations. There is a certain specificity for the HepG2 and MCF7 lines, but only at low calixarene concentrations, which seems to disappear at high macrocycle concentrations.

Cytotoxicity assays were also performed with a normal RPE-1 cell line. The same results as for the cancerous lines were obtained. Overall, these results demonstrate that the Schiff Base calix[4]arene studied can be used as nanovector or nanocarrier in nanomedicine at concentrations up to  $0.32 \mu\text{mol dm}^{-3}$  (~75% cell viability in RPE-1 cells).

#### 4. Conclusions

In conclusion, the Schiff Base calix[4]arene interacts with calf thymus ct-DNA, generating conformational change. At low concentrations of calixarene, the macrocycle binds to the polynucleotide by a groove mode, which induces partial double-strand denaturation. This interaction results in a partial compaction of the ct-DNA: the macromolecule goes from an elongated state (coil) to a more compact one (globule). When the concentration of calixarene increases ( $X > 0.003$ ) decompaction of the polynucleotide is observed. The formation of calixarene aggregates in solution would weaken the calixarene/ct-DNA interaction, thus resulting in the presence of free ct-DNA molecules.

Cytotoxicity data indicate that the Schiff Base calixarene has the potential to be used as nanovector up to  $0.32 \mu\text{mol dm}^{-3}$  (~75% cell viability in RPE-1 cells), as well as nanocarrier for anticancer drugs such as doxorubicin, cytarabine, paclitaxel, among others, as has been demonstrated with other calixarenes [37].



**Author Contributions:** Conceptualization, M.L.-L., P.L.-C. and M.L.M.; methodology, F.J.O., J.A.L., C.B.G.-C., I.V.R., M.L.-L., P.L.-C., E.B., M.D., A.M.-W. and M.L.M.; software, J.A.L., F.J.O. and E.B.; validation, M.L.-L., P.L.-C. and M.L.M.; formal analysis, F.J.O., J.A.L., E.B., M.D., A.M.-W., M.L.-L., P.L.-C., and M.L.M.; investigation, F.J.O., J.A.L., C.B.G.-C., I.V.R., M.D., A.M.-W., E.B., M.L.-L., P.L.-C. and M.L.M.; resources, P.L.-C. and M.L.M.; data curation, F.J.O., J.A.L., E.B., A.M.-W. and M.L.M.; writing—original draft preparation, F.J.O., E.B., M.L.-L., P.L.-C. and M.L.M.; writing—review and editing, F.J.O., M.L.-L., P.L.-C., E.B. and M.L.M.; visualization, F.J.O., M.L.-L., P.L.-C., E.B. and M.L.M.; supervision, F.J.O., M.L.-L., P.L.-C. and M.L.M.; project administration, M.L.-L., P.L.-C. and M.L.M.; funding acquisition, P.L.-C. and M.L.M. All authors have read and agreed to the published version of the manuscript.

**Funding:** This research received no external funding.

**Institutional Review Board Statement:** Not applicable.

**Informed Consent Statement:** Not applicable.

**Data Availability Statement:** Not applicable.

**Acknowledgments:** This work was financed by the Consejería de Conocimiento, Innovación y Universidades de la Junta de Andalucía (FQM-206, FQM-274, and PY20-01234), the VI Plan Propio Universidad de Sevilla (PP2019/00000748), RTI2018-100692-B-100; P18-RT-1271; PI18-0005-2018; VI-PP AY.SUPLEM-2019; RYC-2015-18670 and the European Union (Feder Funds). F.J.O. thanks the University of Seville for the grant VPPI-US (DOC\_00963). J.A.L. also thanks the Fundación ONCE funded by the Fondo Social Europeo.

**Conflicts of Interest:** The authors declare no conflict of interest.

## References

1. Hanna, E.; Rémuzat, C.; Auquier, P.; Toumi, M. Gene Therapies Development: Slow Progress and Promising Prospect. *J. Mark. Access Health Policy* **2017**, *5*, 1265293. [[CrossRef](#)]
2. Choi, J.S.; Joo, D.K.; Kim, C.H.; Kim, K.; Park, J.S. Synthesis of a Barbell-like Triblock Copolymer, Poly(L-Lysine) Dendrimer-Block-Poly(Ethylene Glycol)-Block-Poly(L-Lysine) Dendrimer, and Its Self-Assembly with Plasmid DNA. *J. Am. Chem. Soc.* **2000**, *122*, 474–480. [[CrossRef](#)]
3. Parker, A.L.; Oupicky, D.; Dash, P.R.; Seymour, L.W. Methodologies for Monitoring Nanoparticle Formation by Self-Assembly of DNA with Poly(L-Lysine). *Anal. Biochem.* **2002**, *302*, 75–80. [[CrossRef](#)]
4. Jiménez Blanco, J.L.; Benito, J.M.; Ortiz Mellet, C.; García Fernández, J.M. Molecular Nanoparticle-Based Gene Delivery Systems. *J. Drug Deliv. Sci. Technol.* **2017**, *42*, 18–37. [[CrossRef](#)]
5. Zhou, T.; Llizo, A.; Wang, C.; Xu, G.; Yang, Y. Nanostructure-Induced DNA Condensation. *Nanoscale* **2013**, *5*, 8288–8306. [[CrossRef](#)]
6. Rodik, R.V.; Klymchenko, A.S.; Mely, Y.; Kalchenko, V.I. Calixarenes and Related Macrocycles as Gene Delivery Vehicles. *J. Incl. Phenom. Macrocycl. Chem.* **2014**, *80*, 189–200. [[CrossRef](#)]
7. Sansone, F.; Dudič, M.; Donofrio, G.; Rivetti, C.; Baldini, L.; Casnati, A.; Cellai, S.; Ungaro, R. DNA Condensation and Cell Transfection Properties of Guanidinium Calixarenes: Dependence on Macrocycle Lipophilicity, Size, and Conformation. *J. Am. Chem. Soc.* **2006**, *128*, 14528–14536. [[CrossRef](#)]
8. Rodik, R.V.; Klymchenko, A.S.; Jain, N.; Miroshnichenko, S.I.; Richert, L.; Kalchenko, V.I.; Mély, I. Virus-Sized DNA Nanoparticles for Gene Delivery Based on Micelles of Cationic Calixarenes. *Chem.—Eur. J.* **2011**, *17*, 5526–5538. [[CrossRef](#)]
9. Lalor, R.; DiGesso, J.L.; Mueller, A.; Matthews, S.E. Efficient Gene Transfection with Functionalised Multicalixarenes. *Chem. Commun.* **2007**, *46*, 4907–4909. [[CrossRef](#)]
10. Rullaund, V.; Siragusa, M.; Cumbo, A.; Gygax, D.; Shahgaldian, P. DNA Surface Coating of Calixarene-Based Nanoparticles: A Sequence-Dependent Binding Mechanism. *Chem. Commun.* **2012**, *48*, 12186–12188. [[CrossRef](#)]
11. Zadnád, R.; Schrader, T. DNA Recognition with Large Calixarene Dimers. *Angew. Chem.—Int. Ed.* **2006**, *45*, 2703–2706. [[CrossRef](#)]
12. Blecking, C.J.; Hu, W.; Zadnád, R.; Dasgupta, A.; Schrader, T. A Modular Synthetic Route to Dimeric Calixarenes: A New Family of DNA Major Groove Binders. *Synthesis* **2011**, *2011*, 1193–1204. [[CrossRef](#)]
13. Liu, Y.J.; Chao, H.; Yao, J.H.; Tan, L.F.; Yuan, Y.X.; Ji, L.N. Ruthenium(II) Complexes Containing Asymmetric 2-(Pyrazin-2-Yl) Naphthoimidazole: Syntheses, Characterization, DNA-Binding and Photocleavage Studies. *Inorg. Chim. Acta* **2005**, *358*, 1904–1910. [[CrossRef](#)]
14. Secco, F.; Venturini, M.; Biver, T.; Sánchez, F.; Prado-Gotor, R.; Grueso, E. Solvent Effects on the Kinetics of the Interaction of 1-Pyrenecarboxaldehyde with Calf Thymus DNA. *J. Phys. Chem. B* **2010**, *114*, 4686–4691. [[CrossRef](#)]
15. Saenger, W. *Principles of Nucleic Acid Structure*, 1st ed.; Springer: New York, NY, USA, 1984; p. XX-556.

16. Supian, F.L.; Richardson, T.H.; Deasy, M.; Kelleher, F.; Ward, J.P.; McKee, V. Interaction between Langmuir and Langmuir–Blodgett Films of Two Calix[4]Arenes with Aqueous Copper and Lithium Ions. *Langmuir* **2010**, *26*, 10906–10912. [[CrossRef](#)]
17. Rosa, M.; Dias, R.; Graça Miguel, M.; Lindman, B. DNA–Cationic Surfactant Interactions Are Different for Double- and Single-Stranded DNA. *Biomacromolecules* **2005**, *6*, 2164–2171. [[CrossRef](#)]
18. Van Meerloo, J.; Kaspers, G.J.L.; Cloos, J. Cell Sensitivity Assays: The MTT Assay. In *Cancer Cell Culture. Methods and Protocols*, 2nd ed.; Cree, I.A., Ed.; Humana: Totowa, NJ, USA, 2011; Volume 731, pp. 237–245.
19. Rahban, M.; Divsalar, A.; Saboury, A.A.; Golestani, A. Nanotoxicity and Spectroscopy Studies of Silver Nanoparticle: Calf Thymus DNA and K562 as Targets. *J. Phys. Chem. C* **2010**, *114*, 5798–5803. [[CrossRef](#)]
20. Menger, F.M.; Portnoy, C.E. Chemistry of Reactions Proceeding inside Molecular Aggregates. *J. Am. Chem. Soc.* **1967**, *89*, 4698–4703. [[CrossRef](#)]
21. Moyá, M.L.; Ostos, F.J.; Moreno, I.; García, D.; Moreno-Gordillo, P.; Rosado, I.V.; López-Cornejo, P.; Lebrón, J.A.; López-López, M. Metallo-Liposomes Derived from the [Ru(Bpy)<sub>3</sub>]<sup>2+</sup> Complex as Nanocarriers of Therapeutic Agents. *Chemosensors* **2021**, *9*, 90. [[CrossRef](#)]
22. Berova, N.; Nakanishi, K.; Woody, R.W. *Circular Dichroism. Principles and Applications*, 2nd ed.; John Wiley & Sons: New York, NY, USA, 2000; p. 912.
23. Ostos, F.J.; Lebron, J.A.; Moyá, M.L.; Deasy, M.; López-cornejo, P. Binding of DNA by a Dinitro-Diester Calix[4]Arene: Denaturation and Condensation of DNA. *Colloids Surf. B Biointerfaces* **2015**, *127*, 65–72. [[CrossRef](#)]
24. Lincoln, P.; Broo, A.; Nordén, B. Diastereomeric DNA-Binding Geometries of Intercalated Ruthenium(II) Trischelates Probed by Linear Dichroism. *J. Am. Chem. Soc.* **1996**, *118*, 2644–2653. [[CrossRef](#)]
25. Gatasheh, M.K.; Kannan, S.; Hemalatha, K.; Imrana, N. Proflavine an Acridine DNA Intercalating Agent and Strong Antimicrobial Possessing Potential Properties of Carcinogen. *Karbala Int. J. Mod. Sci.* **2017**, *3*, 272–278. [[CrossRef](#)]
26. Passero, F.; Gabbay, E.J.; Gaffney, B.; Kurucsev, T. Topography of Nucleic Acid Helices in Solutions. Stoichiometry and Specificity of the Interaction of Reporter Molecules with Nucleic Acid Helices. *Macromolecules* **1970**, *3*, 158–162. [[CrossRef](#)]
27. Chaires, J.B. A Thermodynamic Signature for Drug-DNA Binding Mode. *Arch. Biochem. Biophys.* **2006**, *453*, 26–31. [[CrossRef](#)]
28. Nishimura, T.; Okobira, T.; Kelly, A.M.; Shimada, N.; Takeda, Y.; Sakurai, K. DNA Binding of Tilorone: <sup>1</sup>H NMR and Calorimetric Studies of the Intercalation. *Biochemistry* **2007**, *46*, 8156–8163. [[CrossRef](#)] [[PubMed](#)]
29. Hranjec, M.; Lučić, B.; Ratkaj, I.; Pavelić, S.K.; Piantanida, I.; Pavelić, K.; Karminski-Zamola, G. Novel Imidazo[4,5-b]Pyridine and Triaza-Benzo[c]Fluorene Derivatives: Synthesis, Antiproliferative Activity and DNA Binding Studies. *Eur. J. Med. Chem.* **2011**, *46*, 2748–2758. [[CrossRef](#)]
30. Richard, H.; Schreiber, J.P.; Daune, M. Interactions of Metallic Ions with DNA. V. DNA Renaturation Mechanism in the Presence of Cu<sup>2+</sup>. *Biopolymers* **1973**, *12*, 1–10. [[CrossRef](#)]
31. Eichhorn, G.L.; Shin, Y.A. Interaction of Metal Ions with Polynucleotides and Related Compounds. XII. The Relative Effect of Various Metal Ions on DNA Helicity. *J. Am. Chem. Soc.* **1968**, *90*, 7323–7328. [[CrossRef](#)]
32. Supian, F.L.; Richardson, T.H.; Deasy, M.; Kelleher, F.; Ward, J.P.; McKee, V. A Surface Potential Study of Ion-Uptake by 5,11,17,23-Tetra-Tert-Butyl-25,27-Diethoxycarbonyl Methyleneoxy-26,28-Dihydroxycalix[4]Arene and 5,17-(3-Nitrobenzylideneamino)-11,23-Di-Tert-Butyl-25,27-Diethoxycarbonyl Methyleneoxy-26,28-Dihydroxycalix[4]Arene Langmuir Blodgett (LB) Monolayers. *Sains Malays.* **2010**, *39*, 423–433. [[CrossRef](#)]
33. Fang, Y.; Hoh, J.H. Early Intermediates in Spermidine-Induced DNA Condensation on the Surface of Mica. *J. Am. Chem. Soc.* **1998**, *120*, 8903–8909. [[CrossRef](#)]
34. Rau, D.C.; Parsegian, V.A. Direct Measurement of the Intermolecular Forces between Counterion-Condensed DNA Double Helices. Evidence for long range attractive hydration forces. *Biophys. J.* **1992**, *61*, 246–259. [[CrossRef](#)]
35. Grueso, E.; Cerrillos, C.; Hidalgo, J.; Lopez-Cornejo, P. Compaction and Decompaction of DNA Induced by the Cationic Surfactant CTAB. *Langmuir* **2012**, *28*, 10968–10979. [[CrossRef](#)] [[PubMed](#)]
36. García, J.P.; Marrón, E.; Martín, V.I.; Moyá, M.L.; Lopez-Cornejo, P. Conformational Changes of DNA in the Presence of 12-s-12 Gemini Surfactants (S = 2 and 10). Role of the Spacer's Length in the Interaction Surfactant-Polynucleotide. *Colloids Surf. B Biointerfaces* **2014**, *118*, 90–100. [[CrossRef](#)] [[PubMed](#)]
37. Ostos, F.J.; Lebrón, J.A.; Moyá, M.L.; López-López, M.; Sánchez, A.; Clavero, A.; García-Calderón, C.B.; Rosado, I.V.; López-Cornejo, P. P-Sulfocalix[6]Arene as Nanocarrier for Controlled Delivery of Doxorubicin. *Chem.—Asian J.* **2017**, *12*, 679–689. [[CrossRef](#)]